ROYAL SOCIETY
OF CHEMISTRY

COMMUNICATION
Yoichi Okimoto *et al.*
Ultrafast variation of the polarized state in proton-π electron
coupled ferroelectric cocrystal Phz-H_2ca

ROYAL SOCIETY OF CHEMISTRY

Check for updates

Ultrafast variation of the polarized state in proton-π electron coupled ferroelectric cocrystal Phz-H$_2$ca†

Akihiro Sugisawa, [ID]^a Tsugumi Umanodan,^{a} Hongwu Yu, [ID]^a Tadahiko Ishikawa, [ID]^a Shin-ya Koshihara, [ID]^a Sachio Horiuchi [ID]^b and Yoichi Okimoto [ID]$\star^a$

The photoexcitation dynamics of an organic ferroelectric phenazine-chloranilic cocrystal is studied using time-resolved reflectance and second harmonic generation (SHG) measurements. By exciting intramolecular transition, ultrafast variations of reflectivity and SHG are observed, which are discussed based on the scenario of growth of polarization inversion domains proposed theoretically.

Ferroelectrics are a group of polar materials in which an external electric field can reverse the direction of spontaneous polarization. As a result, ferroelectric materials provide us with various practical functions such as storing electricity (capacitors), storing information (memory), and mutually converting mechanical and electrical energy (piezoelectric devices or mechanical actuators). Therefore, ferroelectrics are becoming one of the most important research targets in materials science.

Triggered by the recent development of ultrafast laser techniques, high-speed switching materials have been explored.[1–3] The laser sources generating intense and ultrashort optical pulses from the near-infrared to terahertz wavelength range make it possible to observe the optical response of materials on a timescale of less than 100 fs.[4–8] Ferroelectrics are also a target of such optical control and several examples of ultrafast change of the polarization have been demonstrated in organic and inorganic ferroelectrics.[9–16] Here, we focus on hydrogen-bonded organic ferroelectrics, which have been increasingly developed and studied due to their promising features such as environmental friendliness, flexibility, and plasticity.[17,18]

A target material of this study is a hydrogen-bonded π-molecular cocrystal of a proton acceptor, phenazine (Phz), and a proton donor, chloranilic acid (2,5-dichloro-3,6-dihydroxy-*p*-benzo-

quinone, H$_2$ca). Phz-H$_2$ca is a ferroelectric material with a Curie temperature (T_c) near room temperature (T_c = 253 K).[19] Fig. 1 shows the crystal structure viewed along the *b*-axis. (In Fig. S1 (ESI†), we show a crystal structure diagram when we viewed along the *c*-axis.) There are two hydrogen-bonded chains extending along the crystal [110] and [$\bar{1}$10] directions, respectively. Note that spontaneous polarization appears in the *b*-direction. The reported structural analyses based on X-ray and neutron diffraction data show that asymmetric displacement of protons modulates the intermolecular hydrogen-bonded N–O distances and the charge density of protons below T_c and then has significant contributions to the ferroelectricity.[20] Furthermore, density functional theory calculations considering van der Waals forces have revealed that the Phz-H$_2$ca cocrystal is a displacive ferroelectric in which the proton is the key to its origin.[21]

This paper aims to investigate the dynamics of polarization state changes in the Phz-H$_2$ca cocrystal after photoexcitation on a femtosecond scale. Specifically, we induce intramolecular π–π* transition in H$_2$ca by photoexcitation, then pursue the system's transient changes in reflectivity and second harmonic
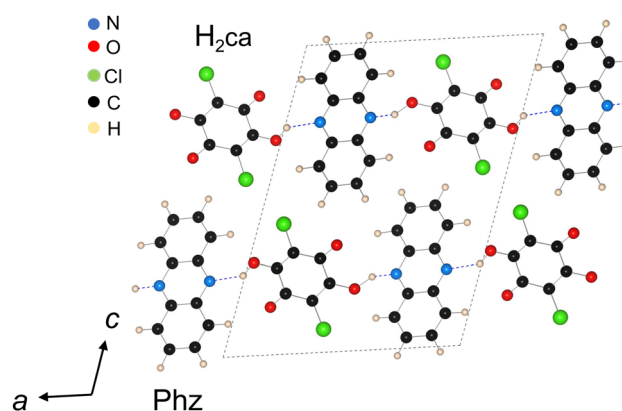
^{a} Department of Chemistry, Tokyo Institute of Technology, Meguro, Tokyo 152-8551, Japan. E-mail: okimoto.y.aa@m.titech.ac.jp

^{b} Research Institute for Advanced Electronics and Photonics (RIAEP), National Institute of Advanced Industrial Science and Technology (AIST), Tsukuba, Ibaraki 305-8565, Japan

Fig. 1 Molecular structures for Phz and H$_2$ca and crystal arrangement viewed along the *b*-axis in the ferroelectric phase.[20]

generation (SHG) with a temporal resolution of approximately 100 fs. The SHG is a second-order nonlinear optical effect that can sensitively probe the degree of the inversion symmetry breaking in the Phz-H_2ca cocrystal. We aim to comprehensively clarify the dynamics of the electronic and polarization states of the system by acquiring the time variations of the reflectivity and SHG.

The single crystal of Phz-H_2ca used in this experiment was grown by diffusion of Phz and H_2ca in an acetone solution, as described in ref. 19. The crystals have a well-developed lustrous (001) surface, and all the optical measurements were performed on that plane. The direction of the crystal axis is determined directly from X-ray crystallography and reflectance anisotropy measurements.

Steady-state reflectivity at a wavelength of 800 nm was measured using monochromatic light obtained from a tungsten lamp through a grating-type monochromator. The sample was fixed in a cryostat and a Si photodiode detected the reflected light to measure the temperature dependence of the 800 nm reflectance.

The relative reflectance change ($\Delta R/R$) and relative SHG intensity change ($\Delta I_{SH}/I_{SH}$) after photoexcitation were measured using the usual pump–probe method. A regenerative amplified mode-locked Ti:sapphire laser (a pulse width of about 100 fs, a repetition rate of 1 kHz, and an energy of 1.55 eV) was used as the light source. First, the pulse from the laser source was split into two pulses using a beam splitter. One was converted into a signal light (1213 nm) using an optical parametric amplifier. Then, a pulse of ≈ 480 nm was generated from the signal and original fundamental pulses through a sum frequency generation process. The fluence of the pump light on the sample surface is ≈ 2.8 mJ cm^{-2}. This wavelength of 480 nm is known to induce intramolecular transitions in H_2ca molecules.[22]

The other 800 nm pulse was used as the probe light for $\Delta R/R$ and $\Delta I_{SH}/I_{SH}$ measurements. Fig. 2 shows the experimental setup used for the pump–probe SHG measurement. The pump
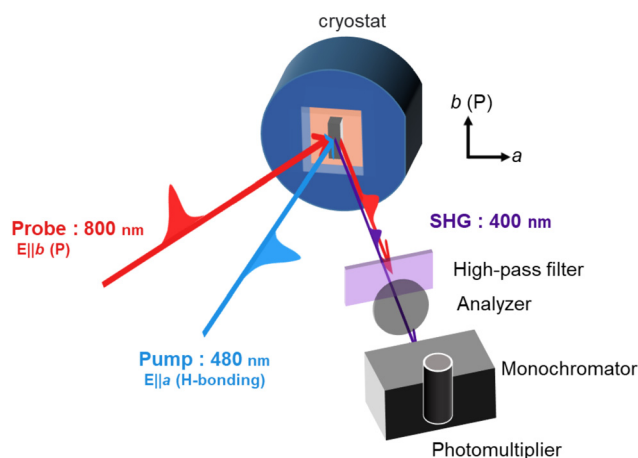

Fig. 2 Experimental setup for the pump–probe SHG measurement. The red and blue pulses denote the probe (800 nm) and pump pulses (480 nm). The Phz-H_2ca crystal was set in a cryostat and generated SHG pulse was detected by using a photomultiplier through a filter and grating monochromator.

light polarization is parallel to the a-axis and the probe light polarization is parallel to the b-axis. More detailed experimental setup diagrams are provided in Fig. S2 (ESI†).

The blue circles in Fig. 3(a) show the temperature dependence of the SHG intensity emitted in the b-axis direction when the sample is cooled from room temperature. SHG intensity suddenly grows upon cooling below T_c, indicating that the degree of symmetry breaking increases in the ferroelectric phase. The red circle in Fig. 3(a) shows the temperature dependence of the reflectance at 800 nm when the sample is cooled from room temperature and incident polarization is along the b-axis. Fig. 3(b) and (c) show the azimuth angle (θ) dependence of the SHG intensity emitted in the a-direction [Fig. 3(b)] and in the b-direction [Fig. 3(c)], measured at 240 K (red circles) and 200 K (blue circles). The angle between the direction of incident polarization and the crystal a-direction defines the value of θ in Fig. 3(b) and (c). As shown in Fig. 3(b) and (c), the angle dependence of SHG shows a quatrefoil shape in Fig. 3(b) and a figure-of-8 shape in Fig. 3(c), indicating anisotropic angle profiles reflecting the crystal orientation. The point group of the Phz-H_2ca cocrystal is 2 in a monoclinic symmetry.[19] We analyzed the angular profile based on this symmetry to understand the azimuth angle dependence of the generated SHG intensity. The components of the contracted tensor of second-order nonlinear susceptibility (d_{ij}) are described as[23]

$$d_{ij} = \begin{pmatrix} 0 & 0 & 0 & d_{14} & 0 & d_{16} \\ d_{21} & d_{22} & d_{23} & 0 & d_{25} & 0 \\ 0 & 0 & 0 & d_{34} & 0 & d_{36} \end{pmatrix}. \quad (1)$$

The a- and b-direction components of the second-order nonlinear polarization (P_a^{NL} and P_b^{NL}) are expressed as $P_a^{NL} \propto d_{16}E^2 \sin 2\theta$ and $P_b^{NL} \propto d_{21}E^2 \cos \theta^2 + d_{22}E^2 \sin \theta^2$, respectively. E represents the electric field intensity of the incident light. The solid lines shown in Fig. 3(b) and (c) are the results of fitting using these relationships at 240 K (red) and 200 K (blue), which reproduce the experimental results well. The tensor component ratios obtained by fitting are $d_{16} : d_{21} : d_{22} = 1 : 0.98 : 6.9$ at 240 K and $1 : 1.0 : 6.9$ at 200 K. It was found that d_{22}, the coefficient representing the SHG emitted in the b- direction with incident b-axis polarized light, was the largest.

At first, we discuss the polarization dynamics of the Phz-H_2ca cocrystal after photoexcitation of the π–π^* transition of the H_2ca molecule.[22] Fig. 4(a)–(d) show the time profiles of $\Delta R/R$ polarized along the b-axis (red circles) and $\Delta I_{SH}/I_{SH}$ (blue circles) at selected temperatures after excitation of a 480 nm pulse. (See also Fig. 2 for the relationship between the direction of polarization of the pump and probe light.) The values $\Delta R/R$ and $\Delta I_{SH}/I_{SH}$ decrease within the pulse width (about 100 fs) immediately after the photoexcitation. This indicates that the intramolecular excitation of the H_2ca molecules instantaneously changes the electronic and polarization states of the system. However, their subsequent relaxation dynamics are different from each other. The reflectivity instantaneously relaxes to almost its original value at all temperatures, whereas the $\Delta I_{SH}/I_{SH}$ value monotonously decreases up to 20 ps. This suppression of SHG
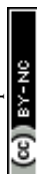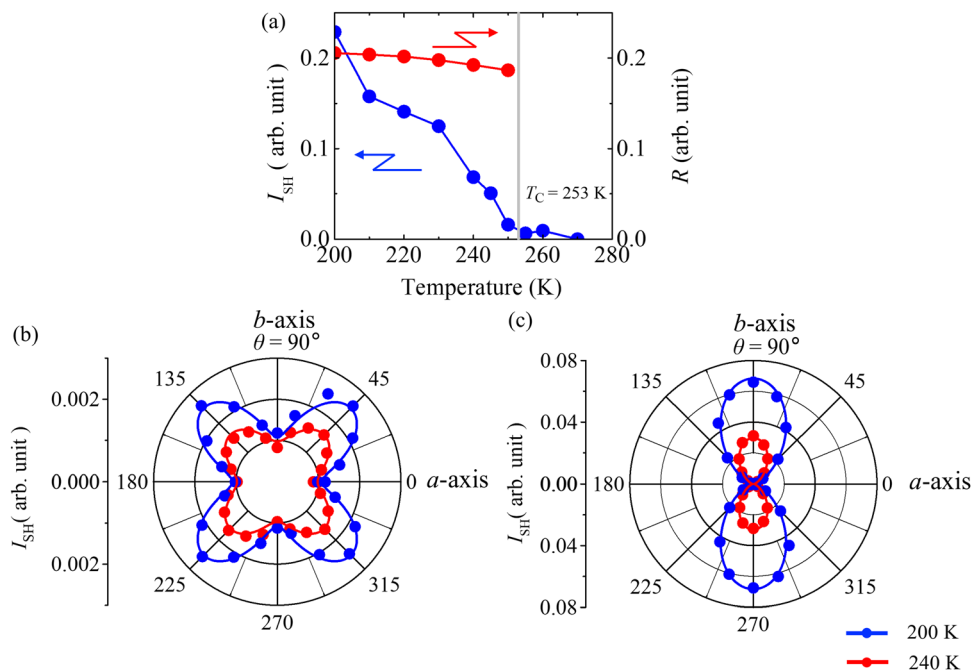
Fig. 3 (a) Temperature dependence of SHG (blue circles) emitted along the b-axis and reflectivity at 800 nm polarized along the b-axis (red circles). (b) and (c) Azimuth angle dependence of SHG emitted along the a-axis (b) and the b-axis (c) at the selected temperature. The solid blue and red curves are fitting results based on point group 2 in a monoclinic structure. (See text).
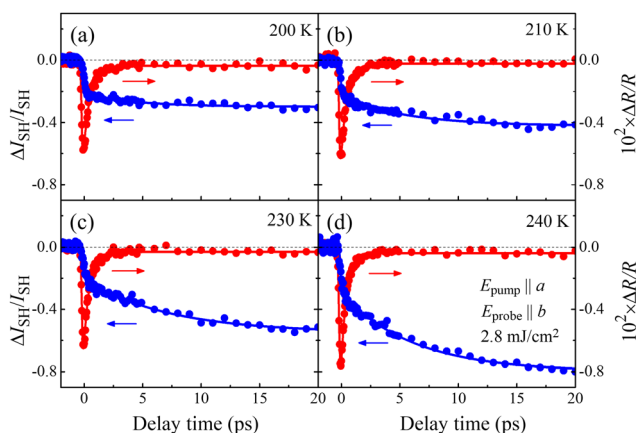

Fig. 4 (a)–(d) Time dependence of relative change of SHG ($\Delta I_{SH}/I_{SH}$, blue circles) and reflectivity at 800 nm ($\Delta R/R$, red circles) after the excitation by a pump pulse. The blue and red lines denote fitting results assuming a single exponential decay. (See text).

is particularly pronounced at 240 K just below T_c, where $\Delta I_{SH}/I_{SH}$ reaches nearly $\approx -80\%$ at 20 ps. Such contrasting time profiles of reflectance and SHG changes are characteristic of this system.

To quantitatively analyse the observed dynamics after photo-excitation, the following functions of $I_R(t)$ and $I_{SH}(t)$ were assumed to represent the temporal changes in reflectance and SHG, respectively:

$$I_R(t) = C_0 \exp\left(-\frac{t}{\tau_1}\right) + C_1, \qquad (2)$$

$$I_{SH}(t) = C_2 + C_3\left\{1 - \exp\left(-\frac{t}{\tau_2}\right)\right\}. \qquad (3)$$

Here, t (> 0) is the delay time, τ_1 and τ_2 are the relaxation times of reflectance and SHG, respectively, and C_0 (C_1) and C_2 (C_3) are constants reflecting the fast (long-lived) components of the reflectance and SHG changes, respectively. The time profiles of $\Delta R/R$ and $\Delta I_{SH}/I_{SH}$ were analyzed based on eqn (2) and (3) (solid curves in Fig. 4) convoluted the device function estimated from the laser pulse. We can reproduce the reflection and SHG profiles well and estimate two relaxation times as $\tau_1 \approx 0.56$ ps and $\tau_2 \approx 6.1$ ps at 240 K.

Based on the analysis of relative reflectance and SHG change, we will discuss the excited state and its relaxation process of the Phz-H$_2$ca cocrystal after photoexcitation. First, a rapid decrease in both reflectance and SHG occurs immediately after photoexcitation. For comparison, the temperature dependence of the reflectance at 800 nm and SHG in the static state of Phz-H$_2$ca is shown in Fig. 3(a). It can be seen that both values decrease with increasing temperature from 200 K toward T_c. Then, one might think that the decrease of the reflectivity and SHG observed immediately after the excitation is due to the temporal heating caused by the laser irradiation. After the sudden decrease, however, the reflectance value increases rapidly with further time at all temperatures, whereas SHG continues to decrease slowly, as can be seen from Fig. 4(a)–(d). These initial dynamics processes cannot be explained by a simple thermal effect alone in an equilibrium state, indicating that we should distinguish the temperature of the excited π electron from that of the proton and lattice affecting SHG.

Regarding the origin of the initial dynamics of SHG, Iwano *et al.* have recently proposed a theoretical framework in a croconic acid crystal, a similar hydrogen-bonded ferroelectric material. According to their theory, photoexcitation of the π-electrons of the molecule modulates the electron potential surface, thereby inducing an intermolecular transfer of protons and resultant ferroelectric domain inversion.[12] This indicates that photoexcitation induces a macroscopic size domain reversal within the photoexcited area. The SHG light generated from the region of reversed polarization cancels out that generated from the original state, resulting in photoinduced suppression of SHG.[24] This scenario can be applied to the similar hydrogen-bonded ferroelectric Phz-H_2ca; the intramolecular excitation modulates the proton and resultant molecular displacements, causing the instantaneous SHG phenomenon shown in Fig. 4. The value of $\Delta I_{SH}/I_{SH}$ just after the photoirradiation at 240 K is $\approx -35\%$. According to the theoretical scenario, the ratio of the inverted area is expressed by $\left(1 - \sqrt{1 + \Delta I_{SH}/I_{SH}}\right)/2$, indicating that the ratio of the photoinduced reversed domain corresponds to $\approx 9.7\%$ of the total polarization before the excitation. By contrast, since macroscopic polarization reversal hardly affects the reflectivity of the crystal, the observed variation of reflectance is attributed to a change in the refractive index of the crystal caused by the intramolecular excitation in H_2ca.

Next, we discuss the relaxation process of this photoinduced polarization reversal state. First, the change in $\Delta R/R$ almost returns to the pre-photoexcited state with a fast relaxation time ($\tau_1 \approx 0.56$ ps), indicating that the electronic state of the excited chloranilic acid molecule relaxes and returns to the initial state. In contrast, $\Delta I_{SH}/I_{SH}$ remains decreasing and does not return to its original value, continuing to decrease further on the time-scale of $\tau_2 \approx 6.1$ ps.

There are two possible origins for this slow but significant decrease in SHG. The first is the gradual heating during the relaxation of the excited π electron systems. The thermal effect promotes fluctuations of the protons in the hydrogen bonds and suppresses the SHG. However, the change in $\Delta R/R$ at 20 ps ($\approx 0.049\%$) is extremely small compared to the temperature change in reflectivity [Fig. 3(a)], making it difficult to explain the 80% decrease of SHG in Fig. 4 by such a simple thermal effect alone.

The second possible origin is the gradual expansion of inverted polarization domains that immediately appeared after photoexcitation. The photoinduced domain nuclei, whose polarization direction is inverted from that of the crystal surroundings, may grow in real space with time. Under these circumstances, the SHG value successively decreases with the expansion, as long as the total sum of the photoinduced inverted domains is less than half of the observed area. At 240 K, according to the previously mentioned relationship, we can estimate that $\approx 18\%$ of the total polarized domains have undergone a further reversal of polarization ≈ 20 ps after the excitation. Notably, the coercive field in Phz-H_2ca, the minimum electric field that can invert the polarized domain, decreases with approaching T_c,[19] which is consistent with the gradual suppression of SHG being more remarkably observed when the
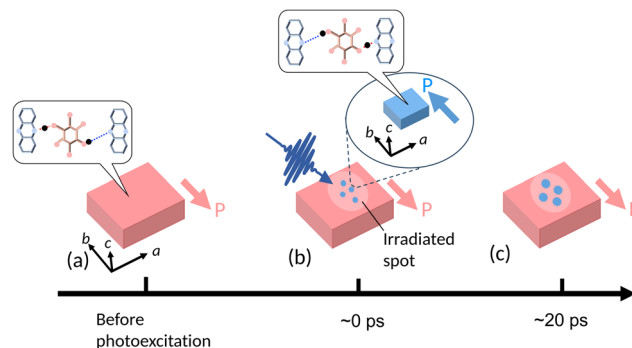

Fig. 5 Schematic illustrations of real space dynamics of Phz-H_2ca crystal. (a) Phz-H_2ca before the excitation, together with Phz and H_2ca molecules. The black circles between the molecules denote protons. The pink rectangle denotes the crystal. (b) The crystal just after the light irradiation (at ≈ 0 ps). The blue islands denote the inverted polarized domains appearing on the surface. The oval area shows the irradiated region of excitation pulses. (c) Expansion of photoinduced domains with elapsing time after the excitation.

temperature approaches T_c. The thermal effect may assist such photoinduced growth of the inverted domain. To confirm it, time-resolved imaging observation of the crystal surface using the SHG microscopy technique[25,26] could shed light, which would be worthy of further study.

Finally, Fig. 5(a)–(c) schematically summarize the proposed polarization domain dynamics driven by photoexcitation of the Phz-H_2ca cocrystal. The original polarized state before excitation is illustrated by the red color [Fig. 5(a)]. Just after the intramolecular excitation of the H_2ca molecule (≈ 0 ps), proton transfer with molecular displacement occurs within the pulse width and macroscopic domains with inverted polarization are generated, as depicted by the blue regions in Fig. 5(b). (As schematically illustrated, the proton represented by the black circle has moved to a different stable point due to photoexcitation than before the excitation, which brings about a successive reversal of the polarization.) While the excited electron rapidly relaxes with a time constant of $\tau_1 \approx 0.56$ ps, the generated polarization reversed domain does not immediately return to its original state, but further expands (Fig. 5(c)) with a time constant of $\tau_2 \approx 6.1$ ps. Such ultrafast domain reversal and gradual expansion of photoinduced polarized regions are characteristic features of the polarization dynamics of the Phz-H_2ca cocrystal.

Conclusions

In conclusion, we investigated the photoexcited dynamics of an organic ferroelectric cocrystal Phz-H_2ca with T_c just below room temperature. The azimuth angle dependence of the SHG confirms that the crystal symmetry is consistent with point group 2; in particular, d_{22} is the dominant tensor component. Pump–probe reflection and SHG measurements with excitation of the intramolecular π–π* transition of H_2ca revealed multi-step dynamics, an instantaneous suppression of reflection and SHG within the laser pulse width and a slow (rapid) relaxation in SHG (reflection). The initial process originates from

macroscopic domain reversal triggered by an intramolecular transition, which has been recently suggested theoretically. The subsequently observed slower relaxation in SHG, which decreases by approximately 80% at 20 ps, is explained by photoinduced growth of polarization reversal domains assisted by thermal effects. This study shows that the polarization structure of hydrogen-bonded organic ferroelectrics can be controlled by photoirradiation, which is expected to pave the way for applications of organic ferroelectrics in ultrafast communication and optical devices, where even higher speeds are required.

Author contributions

Akihiro Sugisawa: investigation, analysis, and original draft preparation. Tsugumi Umanodan: investigation, analysis. Hongwu Yu: investigation. Tadahiko Ishikawa: investigation. Shin-ya Koshihara: reviewing and editing. Sachio Horiuchi: sample preparation, conceptualization. Yoichi Okimoto: conceptualization, supervision, and reviewing and editing.

Conflicts of interest

There are no conflicts to declare.

Acknowledgements

References

1 *Photoinduced Phase Transitions*, ed. K. Nasu, World Scientific, Singapore, 2004.
2 K. Yonemitsu and K. Nasu, *Phys. Rep.*, 2008, **465**, 1–60.
3 S. Koshihara, T. Ishikawa, Y. Okimoto, K. Onda, R. Fukaya, M. Hada, Y. Hayashi, S. Ishihara and T. Luty, *Phys. Rep.*, 2022, **942**, 1–61.
4 T. Morimoto, H. Suzuki, T. Otaki, N. Sono, N. Kida, T. Miyamoto and H. Okamoto, *Phys. Rev. Res.*, 2021, **3**, L04028.
5 N. Kida, T. Miyamoto and H. Okamoto, *J. Phys. Soc. Jpn.*, 2022, **91**, 112011.
6 S. Pal, N. Strkaji, C. Yang, C. Weber, M. Trassin, M. Woerner and M. Fiebig, *Phys. Rev. X*, 2021, **11**, 021023.
7 R. Mankowsky, A. V. Hoegen, M. Först and A. Cavalleri, *Phys. Rev. Lett.*, 2017, **118**, 197601.
8 H. Itoh, H. Obatake, R. Fujiwara, Y. Kawakami, K. Yamamoto, M. Dressei and S. Iwai, *Phys. Rev. Res.*, 2021, **3**, L032043.
9 H. Okamoto, Y. Ishige, S. Tanaka, H. Kishida, S. Iwai and Y. Tokura, *Phys. Rev. B: Condens. Matter Mater. Phys.*, 2004, **70**, 165202.
10 K. Yamamoto, S. Iwai, S. Bokyo, A. Kashiwazaki, F. Hiramatsu, C. Okabe, N. Nishi and K. Yakushi, *J. Phys. Soc. Jpn.*, 2008, **77**, 074709.
11 T. Miyamoto, H. Yada, H. Yamakawa and H. Okamoto, *Nat. Commun.*, 2013, **4**, 2586.
12 K. Iwano, Y. Shimoi, T. Miyamoto, D. Hata, M. Sotome, N. Kida, S. Horiuchi and H. Okamoto, *Phys. Rev. Lett.*, 2017, **118**, 107404.
13 Y. Okimoto, S. Naruse, R. Fukaya, T. Ishikawa, S. Koshihara, K. Oka, M. Azuma, K. Tanaka and H. Hirori, *Phys. Rev. Appl.*, 2017, **7**, 064016.
14 A. V. Hoegen, R. Mankowsky, M. Fechner, M. Först and A. Cavalleri, *Nature*, 2018, **555**, 79–82.
15 T. Umanodan, K. Kaneshima, K. Takeuchi, N. Ishii, J. Itatani, H. Hirori, Y. Sanari, K. Tanaka, Y. Kanemitsu, T. Ishikawa, S. Koshihara, S. Horiuchi and Y. Okimoto, *J. Phys. Soc. Jpn.*, 2019, **88**, 013705.
16 Y. Okimoto, P. Xia, J. Itatani, H. Matsushima, T. Ishikawa, S. Koshihara and S. Horiuchi, *APL Mater.*, 2022, **10**, 090702.
17 A. S. Tayi, A. Kaeser, M. Matsumoto, T. Aida and S. I. Stupp, *Nat. Chem.*, 2015, **7**, 281–294.
18 S. Horiuchi and S. Ishibashi, *J. Phys. Soc. Jpn.*, 2020, **89**, 051009.
19 S. Horiuchi, F. Ishii, R. Kumai, Y. Okimoto, H. Tachibana, N. Nagaosa and Y. Tokura, *Nat. Mater.*, 2005, **4**, 163–166.
20 R. Kumai, S. Horiuchi, H. Sagayama, T. Arima, M. Watanabe, Y. Noda and Y. Tokura, *J. Am. Chem. Soc.*, 2007, **129**, 12920–12921.
21 K. Lee, B. Kolb, T. Thonhauser, D. Vanderbilt and D. Langreth, *Phys. Rev. B: Condens. Matter Mater. Phys.*, 2012, **86**, 104102.
22 R. Kumai, S. Horiuchi and Y. Okimoto, *J. Chem. Phys.*, 2006, **125**, 084715.
23 A. Authier, *International Tables for Crystallography volume D*, Wiley, 2014.
24 T. Umanodan, T. Ishikawa, S. Koshihara, S. Horiuchi and Y. Okimoto, *J. Phys.: Conf. Ser.*, 2019, **1220**, 012012.
25 S. Kumimura and Y. Uesu, *J. Appl. Phys.*, 1997, **81**, 369–375.
26 S. Horiuchi, Y. Tokunaga, G. Giovannetti, S. Picozzi, H. Itoh, R. Shimano, R. Kumai and Y. Tokura, *Nature*, 2010, **463**, 789–792.